Production of nongyrotropic and gyrotropic backstreaming ion distributions in the quasi-perpendicular ion foreshock region

Philippe Savoini, Bertrand Lembège

AGU PUBLICATIONS

JGR

Journal of Geophysical Research: Space Physics

RESEARCH ARTICLE
10.1002/2015JA021018

Key Points:
- Two-dimensional PIC simulations of curved shock recover characteristic escaping populations the ion foreshock
- Collisionless shock front can be the source of field-aligned beams and nongyrotropic population
- E × B drift seems the source of the nongyrotropic backstreaming ions

Correspondence to:
P. Savoini,
Philippe.savoini@upmc.fr

Citation:
Savoini, P., and B. Lembège (2015), Production of nongyrotropic and gyrotropic backstreaming ion distributions in the quasi-perpendicular ion foreshock region, *J. Geophys. Res. Space Physics*, *120*, 7154–7171, doi:10.1002/2015JA021018.

Received 20 JAN 2015
Accepted 22 AUG 2015
Accepted article online 29 AUG 2015
Published online 26 SEP 2015

Production of nongyrotropic and gyrotropic backstreaming ion distributions in the quasi-perpendicular ion foreshock region

Philippe Savoini[1] and Bertrand Lembège[2]

[1]LPP, Ecole Polytechnique-UPMC, Palaiseau, France, [2]LATMOS, Guyancourt, France

Abstract A curved shock is analyzed in the whole quasi-perpendicular propagation region ($90° \geq \theta_{Bn} \geq 45°$) in a supercritical regime with the help of a 2-D particle-in-cell code including self-consistent effects such as the shock front curvature and the time-of-flight effects. Two distinct ion populations are observed within the foreshock: a (gyrotropic) *field-aligned beam* population, hereafter named "FAB," and a (nongyrotropic) *gyrophase bunched* population, hereafter named "GPB." The origin of these high-energy particles and their corresponding acceleration mechanisms are analyzed in details in the present paper. Both FAB and GPB populations are shown to be produced by the shock front itself and more important, do have exactly the same origin. At the shock front, the two populations gain a nongyrotropic distribution, but FAB population loses its initial phase coherency after suffering several bounces along the curved front. This result has one main consequence: the time evolution of the two populations does not involve some distinct reflection processes as often claimed in the literature, but results only from the particle time history at the shock front. This important result was not expected and greatly simplifies the question of their origin. More precisely, a new parameter, the injection angle θ_{inj} has been defined between the shock normal direction and the ion gyrating velocity vector. We found that the FAB population is formed by ions injected almost along the shock front, while GPB population is formed by ions injected almost along the shock normal.

1. Introduction

The foreshock is the region of space magnetically connected to the bow shock that is filled with particles backstreaming from the shock [*Tsurutani and Rodriguez*, 1981; *Paschmann et al.*, 1981; *Bonifazi and Moreno*, 1981a, 1981b; *Fuselier*, 1995; *Eastwood et al.*, 2005; *Oka et al.*, 2005; *Kucharek*, 2008]. In a first approach, the energization of these particles depends strongly on the angle θ_{Bn} defined between the normal to the shock front and the upstream magnetic field, and also, on the Alfven Mach number M_A of the solar wind which determines in fine the amplitude of the potential wall present at the shock front (i.e., the particles acceleration by the parallel electric component). The ion sources of the foreshock are distributed differently over the overall bow shock curvature which allows to distinguish spatial regions of the foreshock populated by different types of ion distributions [see *Eastwood et al.*, 2005, for a review]. Among the different backstreaming ion populations, we will focus on the two distinct groups which are commonly observed within the quasi-perpendicular bow shock region: (i) the field-aligned beam (FAB) ions moving mainly along the foreshock boundary [*Thomsen et al.*, 1983; *Schwartz and Burgess*, 1984; *Oka et al.*, 2005; *Meziane*, 2005] and (ii) the gyrophase bunched (GPB) ions grouped into packets which have the same gyrophase [*Gurgiolo et al.*, 1983; *Thomsen et al.*, 1985; *Meziane et al.*, 2001; *Mazelle et al.*, 2005]. The formation mechanisms of these backstreaming ions have not been clearly established yet and different "scenarios" have been proposed: (i) some of them are based on the guiding center approximation when the magnetic moment is roughly conserved (i.e., adiabatic reflection) [*Sonnerup*, 1969; *Paschmann et al.*, 1980; *Schwartz et al.*, 1983; *Schwartz and Burgess*, 1984], (ii) others invoke on simple geometrical considerations illustrated by the specular reflection [*Gosling et al.*, 1982; *Paschmann et al.*, 1982; *Meziane et al.*, 2011; *Yamauchi et al.*, 2011], and finally others (iii) refer the leakage of some magnetosheath ions which can produce low-energy "FAB" [*Edmiston et al.*, 1982; *Tanaka et al.*, 1983; *Thomsen et al.*, 1983]. Particles diffusion processes have also been invoked to explain such backstreaming populations like (iv) the diffusion of some reflected ions (reflected "gyrating ions") by upstream magnetic fluctuations [*Giacalone et al.*, 1994]

or (v) the ion diffusion which takes place directly within the shock ramp (pitch angle scattering during the reflection process) [*Möbius et al.*, 2001; *Kucharek et al.*, 2004; *Bale et al.*, 2005].

On the other hand, the "GPB" population poses even a greater problem considering their origin. Such ions are observed near the shock front in the quasi-parallel region [*Gosling et al.*, 1982; *Meziane et al.*, 2004a] suffering specular reflection. But these are also observed at some distances from the shock front [*Thomsen et al.*, 1985; *Fuselier et al.*, 1986] and their synchronized nongyrotropic distribution can be explained by low-frequency monochromatic waves trapping [*Mazelle et al.*, 2003; *Hamza et al.*, 2006], or by beam-plasma instabilities [*Hoshino and Terasawa*, 1985] which trap ions and can cause the gyrophase bunched distribution. However, it is quite difficult to discriminate between these different possibilities which can be present simultaneously or separately in time.

In a previous paper, *Savoini et al.* [2013] have used *2-D* particle-in-cell (PIC) simulations where the detailed structures of the shock front are fully involved self-consistently in order to analyze curved shock wave in the quasi-perpendicular domain of propagation (i.e., $45° \leq \theta_{Bn} \leq 90°$) and the associated ion foreshock region. These simulations have recovered the typical FAB and GPB features and associated pitch angle distributions observed experimentally [*Fuselier et al.*, 1986; *Meziane*, 2005]. This work demonstrates that both FAB and GPB populations can be produced by the shock front itself (interaction with macroscopic electric and magnetic fields). Indeed, both populations are mixed together over distances relatively short from the shock front, and do not require any ion instabilities since the simulation time is too short to allow any ion instability to develop in the upstream region. More precisely, the authors have concluded that the FAB population can be associated with long interaction time $\Delta\tilde{t}_{\rm int} > 2\tilde{\tau}_{ci}$ with the shock front where particles move back and forth between the upstream edge of the front and the overshoot (where $\tilde{\tau}_{ci}$ is the ion upstream gyroperiod). During their reflection, these ions form a characteristic gyrotropic perpendicular velocity distribution. In contrast, the ions of the GPB population have a shorter interaction time with the shock front ($\Delta\tilde{t}_{\rm int} \leq 1\tilde{\tau}_{ci}$). Then, if one considers the mechanisms proposed in the literature for the production of the GPB ions, it is appropriate to emphasize the leading role of the electrostatic field present at the ramp as discussed by *Gurgiolo et al.* [1981, 1983] in order to explain their formation in our simulation.

Following this scenario, we presently focus not on the foreshock populations but rather on their respective interaction with the shock front. Then, it is interesting to address three main questions on the reflection mechanism itself: (i) why incoming ions suffer monobounces or multibounces when interacting with the bow shock front, (ii) what features are necessary for these populations to be discriminated when hitting the shock front, and (iii) what is the influence of the shock front nonstationarity on the incoming ions and further backstreaming ions?

These questions will be addressed with the help of a statistical analysis of the backstreaming particles. The paper is organized as follows. In section 2, we briefly describe the self-consistent numerical simulations performed for analyzing a curved supercritical shock propagating within a quasi-perpendicular angular range, and its associated ion foreshock. In section 3, the reflection process is investigated by separating clearly the FAB and GPB populations. Discussion and conclusions will be presented respectively in sections 4 and 5.

2. Numerical Simulation Conditions

The numerical simulation performed in the present paper is similar to that described in *Savoini et al.* [2013]. In short, we used a 2.5 dimensional, fully electromagnetic, relativistic particle code using standard finite-size particle techniques (see *Lembege and Savoini*, 1992, 2002, for planar, and *Savoini and Lembège*, 2001; *Savoini et al.*, 2010, for curved shocks, respectively). In these simulations, fields are separated into electromagnetic transverse components, hereafter denoted by a subscript "*t*," and electrostatic longitudinal components hereafter denoted by a subscript "*l*," which result from the space-charge effects. Nonperiodic conditions are applied along *x*-direction within the simulation box, and periodic conditions are used along *y* direction. Herein, the sizes of the plasma simulation box are $\tilde{L}_x = 6144$ and $\tilde{L}_y = 8192$, which cover 205 and 274 ion inertial lengths ($\tilde{c}/\tilde{\omega}_{pi}$), respectively. With these parameters, the simulation allows to analyze in details a limited upstream region in front of the bow shock. At the end of the simulation, the extent of the ion foreshock is limited to 1.4 the Earth's radius ($D_{\rm foreshock} \approx 1.4R_{\rm Earth}$). All normalized quantities are indicated with a tilde "~."

Table 1. Upstream Numerical Parameters

Parameters	Electrons	Ions
$\tilde{v}_{th}$	0.3	0.026
$\tilde{\lambda}_D$	0.42	0.33
$\tilde{\rho}_c$	0.84	56
$\tilde{c}/\tilde{\omega}_p$	3	30
$\tilde{\omega}_c$	0.5	0.006
$\tilde{\omega}_p$	1	0.1
$\tilde{\tau}_c$	13	1047
$\tilde{\beta}$	0.16	0.10
$\tilde{V}_A$	0.16	0.16

It is important to recall that the magnetostatic field $\vec{B}_o$ is partially lying outside the simulation plane [*Savoini and Lembège*, 2001]. Then, the curvature (roughly half circle) of the generated shock front allows herein a continuous variation of θ_{Bn} from 90° to 45° simulating the whole quasi-perpendicular domain of shock propagation. After a short transient period $\tilde{t} \leq 0.3\tilde{\tau}_{ci}$, the curvature radius $\tilde{R}_c$ of the shock is much larger than the upstream ion Larmor gyroradius $\tilde{\rho}_{ci}$ ($\tilde{R}_c \geq 20\tilde{\rho}_{ci}$). At the end of the simulation, this radius is about $\tilde{R}_c \approx 140\tilde{\rho}_{ci}$. At this stage, we have to point out that the increase of the shock front curvature in time has two distinct consequences: (i) First, as $\tilde{R}_c$ increases, the shock velocity slightly decreases and so, does the Mach Number from $\approx$ 5 to $\approx$ 3, (ii) Second, this includes the well-known time-of-flight effect described in more details by *Savoini and Lembège* [2001]. In short, the time-of-flight effect is a balistic process due to the convection of the upstream magnetic field lines by the incoming solar wind. As a result, backstreaming particles, collected at a given upstream location, come from different parts of the curved shock depending on their respective velocity. In the present solar wind frame, an equivalent situation is obtained since a given upstream magnetic field line connected to the expanding curved shock scans different angles θ_{Bn} with respect to the normal of the shock front.

The time of the simulation is large enough to observe the early stage of the formation of the ion foreshock ($\tilde{t}_{\text{simul}} = 5.3\tilde{\tau}_{ci}$) and to investigate the interaction of incoming ions with the shock front and the formation of resulting backstreaming ions. Initial plasma conditions are summarized as follows: light velocity $\tilde{c} = 3$, temperature ratio between ion and electron population $T_e/T_i = 1.58$. A mass ratio $m_i/m_e = 84$ is used in order to save CPU time and the Alfvèn velocity is $\tilde{v}_A = 0.16$. The shock is in supercritical regime with an Alfvèn Mach number $M_A = \tilde{v}_{\text{shock}}/\tilde{v}_A \approx 4$ measured at $\theta_{Bn} = 90°$ (which is used as a reference angle). All ion and electron plasma parameters are summarized in Table 1.

3. Statistical Point of View on Reflection Processes

Using the criterium on the interaction time range Δt_{int} defined in *Savoini et al.* [2013] to discriminate between the FAB and the GPB populations, we can map the whole ion foreshock region in order to get a general view of both backstreaming populations and to analyze more deeply their respective features. We recall that particles suffering a large interaction time with the shock front (i.e., several local gyroperiod, $\Delta\tilde{t}_{\text{int}} > 2{-}6\tilde{\tau}_{ci}$) are classified as the source of the FAB population. In contrast, particles reflected back after only one bounce at the front (i.e., only one local gyroperiod, $\Delta\tilde{t}_{\text{int}} \approx 1\tilde{\tau}_{ci}$) are classified as the source of the GPB population. For clarifying the presentation, we will split this section into three parts where we analyze respectively (i) the spatial evolution of backstreaming ions in the upstream region, (ii) how the incoming ions interact with the shock front and are backstreaming at later times, and (iii) the reflection processes associated to backstreaming ions.

3.1. Mapping of Backstreaming Ions

For this purpose, we have plotted the density of the FAB and GPB populations (Figure 1) at the end time of the simulation ($\tilde{T} = 5.3\tilde{\tau}_{ci}$).

For reference, we have plotted the location of the curved shock front and the global shape of the whole ion foreshock (thick black lines) where all backstreaming ions have been detected. Let us point out that the lack of particles near the shock front is due to the fact that we have removed all reflected "gyrating" ions. Indeed, in this area, it is impossible to discriminate between the reflected gyrating ions which will go into the downstream region after one gyration and the newly reflected ions which will later escape (backstream) into the upstream region. Our results clearly show that the FAB ions populate the whole foreshock region, extending from the leading edge of the foreshock (indicated by the line starting from $\theta_{Bn} = \theta^{\text{FAB}}_{io,\text{fore}} \approx 66°$) to the deeper foreshock (i.e., until $\theta_{Bn} = 45°$ in our simulation) [*Savoini et al.*, 2013]. In contrast, no GPB ions are observed at and around the edge of the ion foreshock region but are present more deeply within the foreshock (indicated by the dotted line starting from $\theta^{\text{GPB}}_{io,\text{fore}} \leq 62°$ in our results). This defines a thin region where FAB is

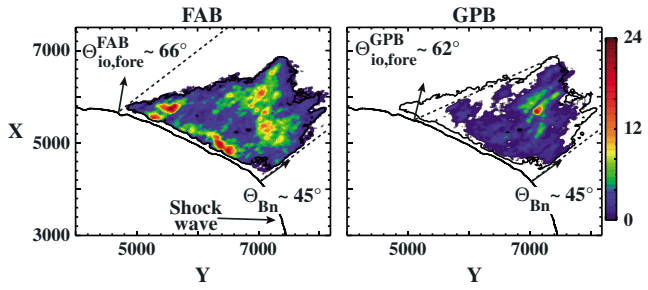

Figure 1. Ion density in the ion foreshock region measured at the end of the simulation $\tilde{T} = 5.3\tilde{\tau}_{ci}$ in an enlarged view of the shock wave. The (left) FAB and (right) GPB populations. The location of the curved shock front, the perimeter of the ion foreshock (black thin lines) and straight (black dashed) lines illustrating the upstream edges for each population foreshock (defined from the angle directions $\theta_{Bn} = 66°$ for the FAB and 62° for the GPB population, respectively) have been plotted as references.

observed without associated GPB which is in agreement with experimental observation data [*Eastwood et al.*, 2005; *Mazelle et al.*, 2005]. The density of the GPB population is globally lower than that of FAB population. The difference between the two populations can be explained by the reflection process itself; indeed, parallel energy gain is increasing with the number of bounces [see *Savoini et al.*, 2013, for more details].

More important, the density (both for FAB and GPB) turns out to be not spatially uniform when moving along the curved shock front and as the distance from the front increases upstream.

1. *Along the bow shock front*, the density colors vary from deep blue ($n \approx 0$) at the edge of the foreshock (i.e., $\theta_{Bn} \approx 66°$) to red ($n \approx 24$) at the quasi-perpendicular position (i.e., $\theta_{Bn} \approx 50°$), apart near the edge of the foreshock which evidences a bursty increase of the reflected ions. Such results recover essentially the density dependence versus θ_{Bn} [*Leroy and Mangeney*, 1984] where the shock front acts as a reflecting magnetic wall. Theoretically, the density increasing computed between $\theta_{Bn} \approx 66°$ to 50° is about 35 to compare to our 24 value. Clearly, this is not the case for the additional localized ion density increase (density bump) observed at the edge of the foreshock. Such a reflection is localized both in space and in time and then is, very difficult to evidence observationally. Indeed, the well-known θ_{Bn} geometrical dependency is strongly related to two assumptions which oversimplifies the bow shock. Namely, the stationarity (in time) and the uniformity (in space) of the shock front are in contrast with the established feature of the front nonstationarity/uniformity evidenced both in many simulations [*Lembege and Dawson*, 1987; *Lembege and Savoini*, 1992; *Lee and Chapman*, 2005; *Scholer and Matsukiyo*, 2004] and experimental results [*Horbury et al.*, 2001; *Moullard et al.*, 2006; *Lobzin et al.*, 2007; *Lefebvre et al.*, 2010; *Mazelle et al.*, 2010]. Considering such drastic approximations, the local reflection conditions are not the same everywhere and can explain this strong increase of escaping ions near 65°. On the other hand, near $\theta_{Bn} \approx 45°$, the lack of reflected ions is due to our choice to remove all reflected gyrating ions (which come back and penetrated the downstream region after only one gyration) in order to be sure that our statistical studies include only backstreaming ions foreshock. Unfortunately, around this angle, the reflected gyrating ions go further upstream, and we need to remove more ions here than in other parts along the bow shock (we are aware that in this case, we have also removed some foreshock ion but it was mandatory to observe herein only backstreaming ions in our foreshock distribution functions).
2. *Along a magnetic field line* (i.e., moving further away from the shock), results were not expected. Indeed, if the bow shock acts as a reflecting magnetic wall, the reflection rate has to be constant in time leading to a uniform reflected ion density. But, this feature is not observed in present results. In contrast, we evidence two distinct regions almost aligned along the curved shock front, characterized by an higher ion density separated by an area where the density reaches minimum (less than one sixth of the maximal density value).

Then, Figure 1 suggests that the reflection process is not uniform in space or in time but this question will not be addressed in this paper since a detailed analysis of individual particles trajectory is necessary which is out of scope of this paper.

Nevertheless, a nonstationarity is also evidenced in the ion reflection process as illustrated in Figure 2a which plots the spatial locations of FAB ions just in front of the shock front at the end of the simulation (at $\tilde{T} = 5.3\tilde{\tau}_{ci}$)

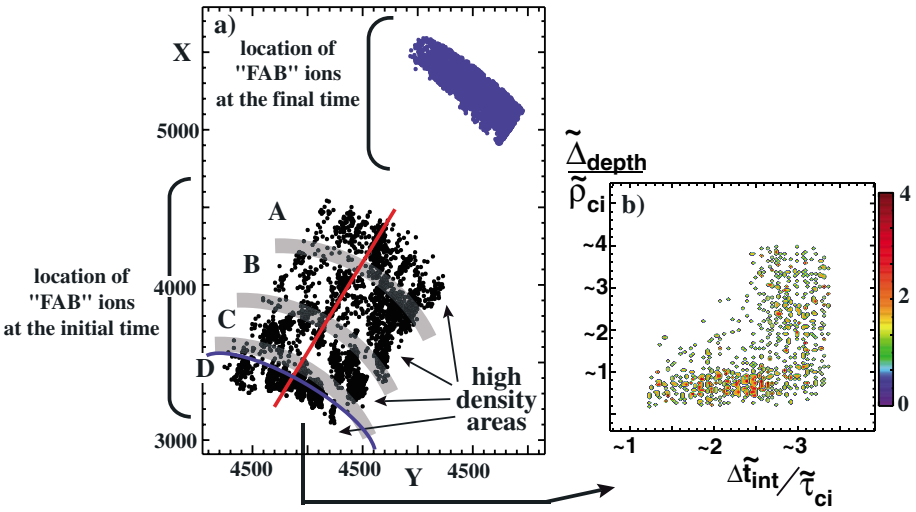

Figure 2. (a) The enlarged view of the *XY* simulation plane where FAB ions defined only in box 2 (see Figure 4 for reference) have been plotted in black dots at the beginning of the simulation (i.e., before their interaction with the shock front) and in blue dots at the end of the simulation (i.e., as these are backstreaming into the upstream region). (b) The shock interaction time $\Delta\tilde{t}_{int}$ versus the penetration depth $\tilde{L}_{depth}$ of the sample "D" of ions defined in the lower part of panel a (below the blue line). The penetration depth $\tilde{L}_{depth}$ and the interaction time $\Delta\tilde{t}_{int}$ are respectively normalized to the upstream ion gyroradius $\tilde{\rho}_{ci}^{upstream}$, and to the upstream ion gyroperiod $\tilde{\tau}_{ci}$.

and of the same FAB ions as these were at the beginning of the simulation (at $\tilde{T} = 0$). We choose all FAB ions defined in the box 2 of Figure 4 (around $\theta_{Bn} \approx 55°$) for two reasons: first, we need to collect enough particles to obtain a good statistic (other locations near the front provide exactly the same result but are not shown here) and second, we wish to leave enough time for the reflected ions to interact with the shock front (i.e., to suffer possible multibounces).

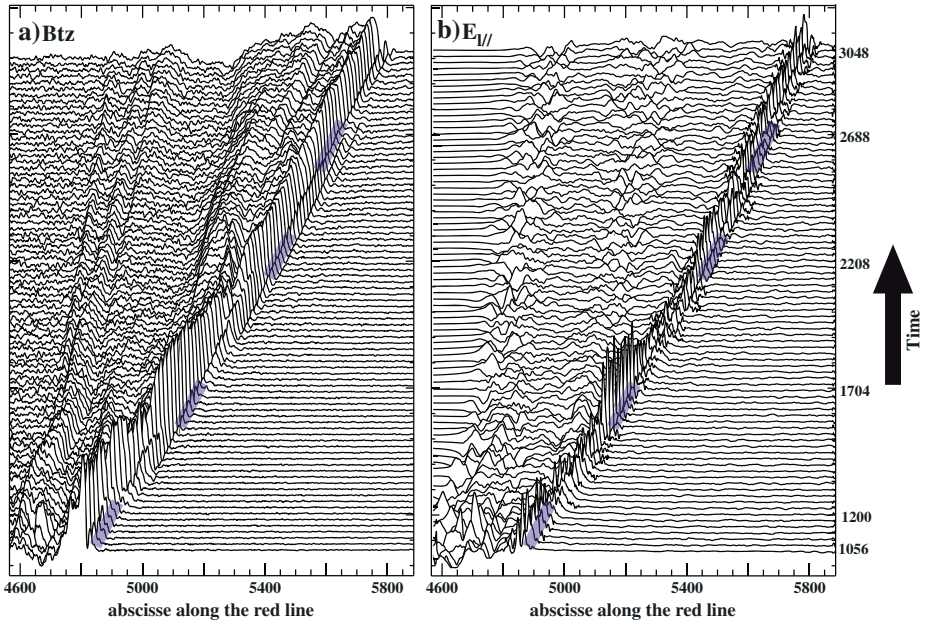

Figure 3. (a) Stackplots of the magnetic field component B_{tz} from $\tilde{t} = 1056$ to 3048 covering the shock interaction time of the different areas (black dots) of Figure 2a. The different curves have been computed along the red thick line shown in Figure 2a. The shock is propagating from the left to the right-hand side and the time interval between two successive curves is $\tilde{t} = 24$. (b) Stackplots of the parallel electric field component El_{para} in the same format of Figure 3a. The thick blue lines represents the different time periods where the magnetic foot/whistler precursor (defined upstream of the ramp) has a weak amplitude (Figure 3a) which corresponds to the different time periods where the amplitude of $E_{l\|}$ component is very large.

This figure shows that the FAB population spreads over a large area before interacting with the shock front. In other words, ions which reach finally the same place (i.e., box 2) are interacting with the shock during few gyroperiods (the shock will need about $3\tau_{ci}^{upstream}$ to sweep the whole area until the ending time).

The initial locations of the "future" FAB ions is nonuniform in space (see fine arrows in Figure 2a), we can identify about four high-density areas aligned along the curved shock front which are separated by low-density areas, marked by thick grey lines on the plot. We are in the solar wind rest reference frame in which the shock propagates and sweeps the upstream region where reflected ions are located. Such nonuniformity in space is due to a nonstationary reflection process (reflection rate is time varying).

This time dependance may have two different origins: (i) The reflection rate may be not constant in time (formation of ions bursts) corresponding to the number of bounces suffered by the particles. This scenario implies that all ions suffering the same number of bounces escape at the same time into the upstream region. In other words, the different high-density areas may be composed of ions having suffered the same number of bounces; (ii) another origin can be the impact of the shock front nonstationarity on the back streaming ions. Indeed, at a particular time, upstream ions may meet appropriate conditions (in terms of local electric and magnetic fields) to be reflected. This nonstationarity of the shock front is now a well-established feature of the supercritical bow shock which may have different underlying mechanisms [see, for example, *Lembege et al.*, 2004, for a review].

In order to discriminate between these two scenarios, we have reported on Figure 2b, the interaction time versus penetration depth of ions belonging to the lowest high-density area observed in Figure 2a (i.e., the area "D," below the blue line). The interaction time range varies from $1.5\tilde{\tau}_{ci}$ to $3.5\tilde{\tau}_{ci}$ and shows that these collected backstreaming ions have suffered from $N_{\text{bounces}} \approx 2$ bounces for ions which hit the shock front at later times till $N_{\text{bounces}} \approx 5$ for ions which hit the shock front earlier, respectively (the time interval between each bounce is $\approx 0.5\tilde{\tau}_{ci}$ which corresponds to one half ion gyration in the upstream region). Then, this high-density area "D" evidences that FAB particles are released independently of their number of bounces and may depend only on the shock dynamic itself. Let us note that we obtain exactly the same result for the other areas, except the last one "A" (further away from the shock front) where ions do not have enough time to suffer several bounces before the end time of the simulation.

This second scenario can be also tested with the help of the stackplots of Figure 3 which show the main magnetic component B_{tz} (Figure 3a) and the parallel electric field (Figure 3b) versus distance for different times extending from $\tilde{t} = 1056$ to 3048 (i.e., covering the time range where the shock front has swept all ions of Figure 2a). The different curves have been plotted along the red thick line of Figure 2a and the shock is propagating from the left-hand to the right-hand side on this plot. Time interval between two successive curves is $\Delta\tilde{t} = 24$.

Different mechanisms responsible for the shock front nonstationarity have been identified, where some lead to large periodic fluctuations of macroscopic fields at the shock front [*Lembege et al.*, 2004]. The analysis of these mechanisms applied to the present curved shock is left a further work. Nevertheless, we can identify several time periods that the magnetic foot/the whistler emitted from the ramp becomes so large that it reached the overshoot amplitude (these time periods are reported with the help of the thick blue lines in Figure 3). During these periods as evidenced by Figure 3b which has the same format as Figure 3a, the local parallel electric field inside the ramp is the highest (i.e., the shock front width is smallest) and large part of ions can be more easily reflected. In contrast, when the amplitude of the magnetic foot/emitted whistler is small or around the half of the overshoot value, the parallel electric component decreases drastically and no backstreaming ions are observed.

In other words, the reflection rate is not constant in time and the ion emission bursts confirms that there is a particular time for which a large part of ions may be reflected by the shock before being released upstream. This behavior is much more difficult to evidence for the GPB population (not shown here) because these ions suffer only one bounce and it is not possible to discriminate between the two scenarios. Nevertheless, we observe that the GPB population (not shown herein) is released into the upstream region at the same time as for the last FAB population (pack "A" in Figure 2a) which indicates that the same process can be invoked for both populations.

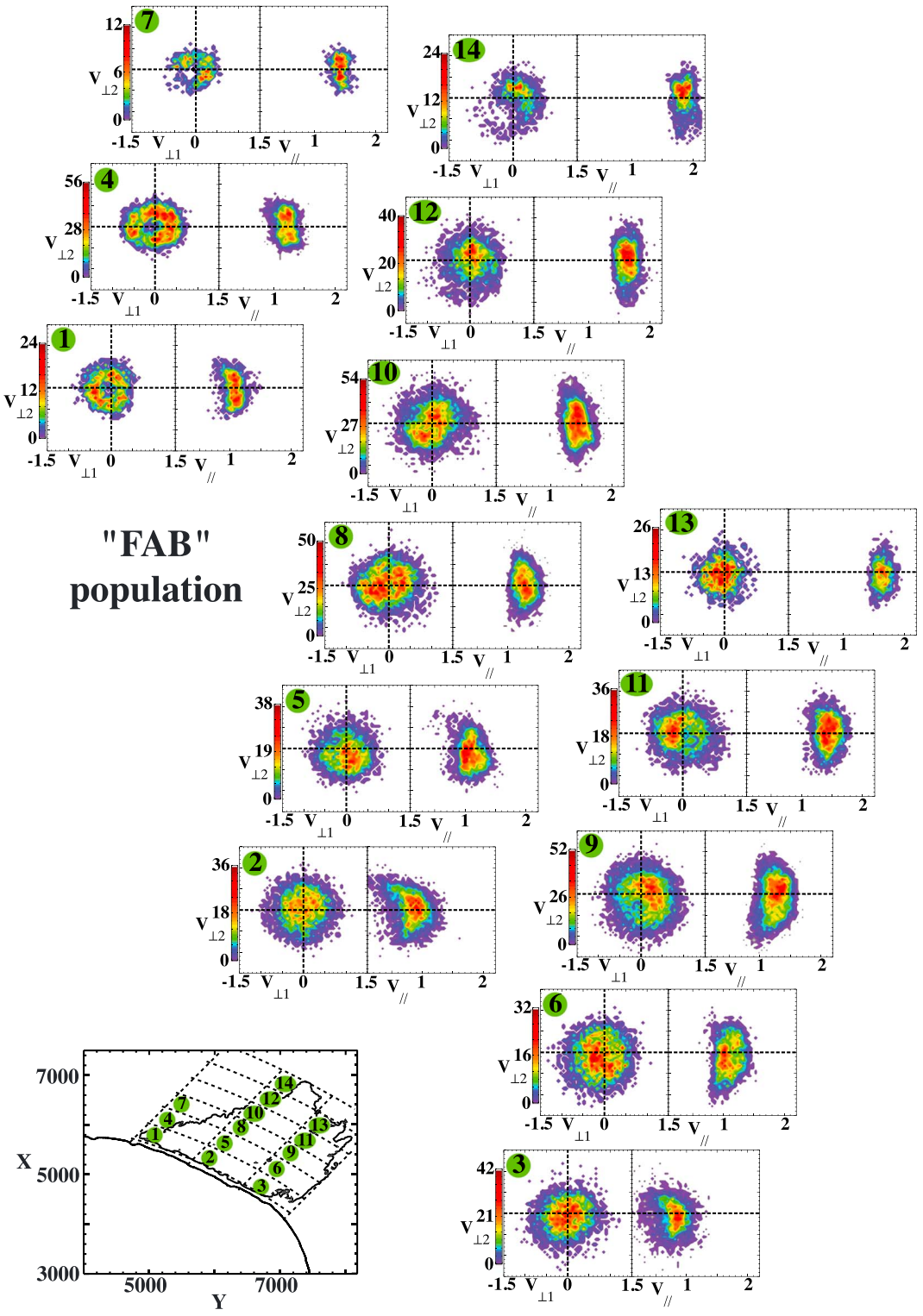

Figure 4. Global mapping of the local FAB ion velocity distribution measured in the foreshock region (only backstreaming ions are selected, the solar wind is excluded). This population has been selected according to their interaction time $\Delta\tilde{t}_{\mathrm{int}}$ (D_{inter}) with the shock front (to see the text). The foreshock region has been divided into local (numbered) sampling boxes aligned along the curved shock front, as shown in the lower part of this figure; all boxes have same shape and same sizes. Two different distributions ($\tilde{v}_{\perp 1}, \tilde{v}_{\perp 2}$) and ($\tilde{v}_{\parallel}, \tilde{v}_{\perp 2}$) are plotted in left and right, respectively, for each sampling box.

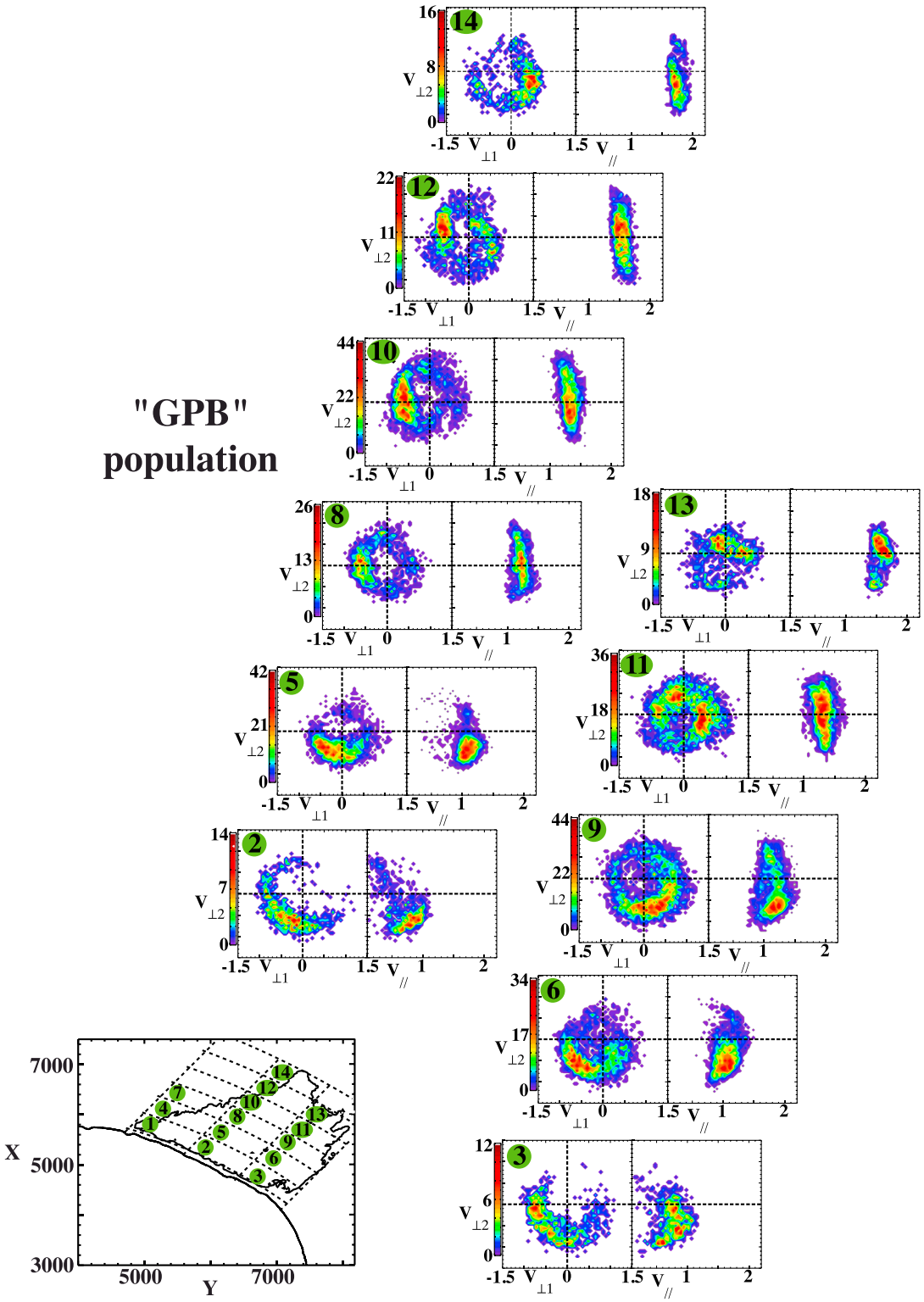

Figure 5. Same as Figure 4 but for GPB ions.

3.2. Velocity Space of Backstreaming Ions

In order to analyze in details the dynamics of backstreaming ions, the overall foreshock area of Figure 1 has been divided into sampling boxes within which local ($\tilde{v}_{\parallel}$ - $\tilde{v}_{\perp 2}$) and ($\tilde{v}_{\perp 1}$ - $\tilde{v}_{\perp 2}$) ion distributions are computed. The size of each sampling box has been chosen to be small enough to follow the progressive changes in local distribution (both in local angle θ_{Bn} and in distance from the shock front) but large enough to satisfy some reasonable statistics. The sampling boxes are aligned along the magnetic field lines projected within the simulation plane as shown in Figures 4 and 5 in order to keep the same shape and the same sizes. Only sampling boxes collecting enough particles in our statistics are taken into account and reported herein. The boxes from 1 to 3 are located along the shock front, whereas the numbers of the other boxes increase when moving further from the shock front and more deeply into the foreshock. Then, at the end time of the simulation, we can identify roughly three different angular ranges: (i) $59° \leq \theta_{Bn} < 66°$ for boxes 1, 4, and 7; (ii) $52° \leq \theta_{Bn} < 59°$ for boxes 2, 5, 8, 10, 12, and 14; and (iii), $45° \leq \theta_{Bn} < 52°$ for boxes 3, 6, 9, 11 and 13. With the help of these sampling boxes, we manage to establish a global map of the ($\tilde{v}_{\perp 2}, \tilde{v}_{\parallel}$) and ($\tilde{v}_{\perp 1}, \tilde{v}_{\perp 2}$) velocity distributions for the FAB and GPB populations in Figures 4 and 5, respectively. The three directions $\parallel$, $\perp_1$, and $\perp_2$ are defined versus the local magnetic field. FAB and GPB populations have been defined versus their shock interaction time as mentioned in section 1. The main relevant features can be summarized as follows:

3.2.1. The FAB Population

In Figure 4, boxes 1, 4, and 7 are populated by reflected ions which are localized along the upstream edge of the ion foreshock. These particles already described in a previous paper [*Savoini et al.*, 2013] have been classified as FAB, even if we observe a small depletion centered around $\tilde{v}_{\perp} \approx 0$ which is not present in so called FAB characteristics. Indeed, these form a gyrotropic distribution characterized by a clear ring in the perpendicular velocity distribution ($\tilde{v}_{\perp 1}, \tilde{v}_{\perp 2}$), which indicates that particles have a random gyrophase. As detailed in the section 3.3, such a distribution can be easily understood if we remember that these boxes collect ions freshly reflected by the shock front (e.g., the shock reaches their position only at the end of the simulation) and so, no many bounces are expected. In other words, these represent an intermediate state of the backstreaming FAB population where ions have suffered too few bounces to lose their initial $\vec{E} \times \vec{B}$ nonzero pitch angle [*Gurgiolo et al.*, 1981, 1983] but enough bounces to have already a gyrotropic distribution function.

When moving more deeply into the ion foreshock (boxes $5-14$), the features of the FAB velocity distributions are well recovered. A perpendicular Maxwellian distribution centered around $\tilde{v} = 0$ is associated to a parallel distribution function, where the parallel bulk velocity increases from $\tilde{v}_{\parallel} \approx 0.8$ near the shock front (Figure 4, boxes $1-3$) to $\tilde{v}_{\parallel} \approx 1.9$ (Figure 4, boxes 13 and 14), when moving further from the shock front. At this stage, we have to point out that it is not the *usual velocity filtering effect* where the fastest particles separate from the slowest ones. Indeed, this velocity filter is an illustration of the different reflection conditions met by the upstream ions when these hit the shock front. In other words, the furthest backstreaming ions in our simulation are ions which have interacted with the shock front earlier in time when the Mach number was higher (i.e., Mach number slowly decreases in time) and then, have gained largest parallel energy.

Finally, we observe the well-known geometrical dependence of the ion parallel velocity with θ_{Bn} when moving along the shock front (boxes $1-3$). If one takes the red area for reference (where the density of ions is maximum), we see that the parallel velocity increases with θ_{Bn} from $v_{\text{para}} \approx 0.8$ near $\theta_{Bn} \approx 45°$ to $v_{\text{para}} \approx 1.1$ near $\theta_{Bn} \approx 66°$, respectively. Then, the ratio of this two velocities is about 1.4, whereas, theoretically if one considers the $\cos(\theta_{Bn})$ dependence, we obtain a ratio of 1.7 between $\theta_{Bn} = 66°$ and $45°$, in a reasonable agreement with our ratio.

3.2.2. The GPB Population

In the same format as Figure 4, Figure 5 plots the local GPB ion distributions observed within the foreshock region. We recall that no a priori hypothesis has been used on their velocity/energy properties and these ions have been only selected by their interaction time with the shock front (i.e., $\Delta t_{\text{int}} \leq 1\tilde{\tau}_{ci}$). The following points can be emphasized:

1. It is worth noting that local ($\tilde{v}_{\perp 1} - \tilde{v}_{\perp 2}$) distributions measured in boxes 2 and 3 are almost the same and present the same bunch of gyrophase angles in the lower left section of the perpendicular velocity distribution. Indeed, the shock front gives to the backstreaming ions exactly the same phase angle around the upstream magnetic field, independently of their initial position along the shock front (i.e., for different θ_{Bn}). This is especially true with our local sampling boxes whose width covers more than $\delta\theta_{Bn} = 7°$ angular range. Indeed, any difference in their perpendicular phase angle would lead to a gyrotropic distribution which is not the case here. This result is in agreement with the mechanism proposed in the literature [i.e., the $\vec{E} \times \vec{B}$

drift of the whole ion distribution *Gurgiolo et al.*, 1981, 1983] which emphasizes the important role of the electrostatic field present at the ramp. Of course, the amplitude of the electric field varies slowly in time and in space along the shock front which can account for the partial diffusion observed in the perpendicular velocity space in these two boxes. Moving further from the shock front (boxes 2 to 14 and 3 to 11) corresponds to particles having left the front at earlier times in the simulation; then, nongyrotropic distributions are not at the same place within the $(\tilde{v}_{\perp 1} - \tilde{v}_{\perp 2})$ space, since particles rotate in the clockwise direction at the upstream gyrofrequency.

2. At the end of the simulation, it is surprising to find relative well-defined nongyrotropic distributions (e.g., boxes 13 and 14 of Figure 5) if we remember that the size of the sampling boxes is relatively large (to obtain good statistics), but can lead to a phase mixing during the time integration of perpendicular velocity. Indeed, when ions are reflected back, they have a nongyrotropic distribution localized in the perpendicular velocity space (see boxes 2 and 3) and rotate in this space at the ω_{ci} gyrofrequency. Of course, if all particles have exactly the same parallel velocity, these would stay in phase as they move further from the shock front. Nevertheless, if now, particles have a parallel velocity along the magnetic field with a nonzero width distribution (which is always the case, as shown in Figure 5), the contribution of particles with different phases $\phi = \omega_{ci} t + \varphi_\circ$ where $\varphi_\circ$ is the initial phase of the particle and ω_{ci} the upstream gyrofrequency, has to be taken into account within a given sampling box. These differences are due to the time required to travel from the shock front to the sampling box (i.e., another illustration of the time-of-flight effects). Then, the absence of such phase mixing in Figure 5 can be explained either (i) by a mechanism which imposes the same perpendicular velocity to all particles (i.e., imposes the same velocity phase) or (ii) by the fact that particles do not have enough time to diffuse in the velocity space.

   In order to clarify this question, we assume the following arguments: first, let us recall that no ion instabilities can be excited during the time length of the simulation; then, one takes into account only the time-of-flight effects and the width of the parallel distribution of reflected ions. Second, we assume that the shock front continuously reflects incoming ions at the same rate (we know that it is not the case but in a first approach this hypothesis greatly simplifies the present argumentation). Then, let us consider a distance D from the shock, where D is measured along the interplanetary magnetic field (*IMF*) projection into the (X, Y) simulation plane. As a consequence, the time for a particle to reach this distance D is $\tau = \frac{D}{v_\parallel}$ and meanwhile, it undergoes a cyclotron motion. Then, its phase is shifted by an angle $\phi = \omega_{ci} \frac{D}{v_\parallel} + \varphi_\circ$. Obviously, particles observed at D will have a different phase ϕ depending of their parallel velocity $v_\parallel$, and a mixing will result.

   In order to estimate the extent of this phase mixing, we can use the following criterion: for a parallel distribution, we can define a minimum $v_{\parallel \min}$ and a maximum $v_{\parallel \max}$ values. Furthermore, we consider that the phase mixing is clearly visible when the relative phase shift is about π (a value of 2π does not change the nongyrotropic distribution).

   We obtain the phase shift relation

$$\omega_{ci} \left(\frac{D}{v_{\parallel \min}} - \frac{D}{v_{\parallel \max}} \right) = \pi \tag{1}$$

   Then, it is simple to estimate the distance D:

$$D = \frac{\pi}{\omega_{ci}} \left(\frac{v_{\parallel \min} v_{\parallel \max}}{v_{\parallel \max} - v_{\parallel \min}} \right) \tag{2}$$

   By writing $v_{\parallel \max} = v_{\parallel \min} + \delta v_\parallel$ and assuming that $\delta v_\parallel \leq v_{\parallel \min}$, we obtain an rough estimate of the distance D dependency as

$$D \propto \frac{v_{\parallel \min}^2}{\delta v_\parallel} \tag{3}$$

   This result emphasizes that larger parallel velocity $v_{\parallel \min}$ preserves the phase coherency over the distance D. This behavior is even amplified by *the velocity filtering effect* (see section 3.2.1 for more details) where only the most energetic ions (highest $v_{\parallel \min}$) can be observed at large distances from the shock front. Consequently, lower $v_{\parallel \min}$ values lead to more diffuse perpendicular distribution; in contrast, higher $v_{\parallel \min}$ values help to the survival of bunched distributions which have not enough time to strongly diffuse. This behavior can explain the nongyrotropic distributions observed in boxes 2 and 3 of Figure 5, whereas these boxes are

populated by "new" born backstreaming ions. Indeed, the values $v_{\parallel min}$ and $v_{\parallel max}$ have to be representative of a large fraction of the backstreaming population and then, are determined in Figure 5 (box 2) from the (yellow) colored isocontour in the $v_{\parallel} - v_{\perp 2}$ distribution (we choose box 2 as reference, but all boxes give approximately the same result). We have $v_{\parallel min} \approx 0.5$ and $\delta v \approx 0.5$, i.e., a π phase mixing after $D = 500$, which is of the order of the boxes size along the projected upstream *IMF* ($L_{\parallel box} \approx 550$). Then, some diffusion can take place over such short distances. When moving more deeply into the foreshock (boxes 5 − 14), the fast increase of $v_{\parallel min} \geq 1$ with a constant $\delta v \approx 0.5$, reduces the phase mixing since we have $D \approx 3000 \approx 1.6\ R_E$ (from equation (3)) which is larger than our present ion foreshock region $D^{max}_{ionforeshock} \approx 2700 \approx 1.4\ R_E$. This dependance versus the initial $v_{\parallel}$ velocity explains easily why bunched perpendicular distributions can be always observed further from the shock front in present results. Of course, these conclusions depend strongly on the reflection process itself which is nonstationary (i.e., depending on the fluctuating shock front) and explain the "donuts" shape observed in the GPB distributions when we take into account all particles (including the "blue" ring) as described in the next section.

3.3. The Reflection Process

The simultaneous evidence of FAB and GPB populations within the foreshock leads to the conclusion that both populations are generated by the shock front itself [*Savoini et al.*, 2013]. Both consist of ions collimated along the *IMF* and their characteristics are very similar in terms of energy and $v_{\parallel}$ distribution. However, their pitch angle and their perpendicular velocity distribution strongly differ and can provide additional informations on their respective origins. The pitch angle (defined between the local magnetic field and the velocity vector in Figure 6a) clearly separates the two populations: (i) the FAB distribution (Figure 6b) is characterized by a maximum around $\alpha \approx 0°$ which decreases rapidly as α increases (i.e., field-aligned beams are gyrotropic); (ii) in contrast, the GPB distribution (Figure 6c) exhibits a maximum for a finite pitch angle, usually around $\alpha \approx 20° - 40°$ and more important, no particles are observed at $\alpha \approx 0°$ (i.e., the whole bunched population rotates around the magnetic field).

With the help of only one criterion (Δt_{int}), we manage to separate the two populations without any simplifying assumptions and then, can investigate how they are generated by the shock front. Herein, we measure the pitch angle of the "future" ion foreshock particles (FAB and GPB are separated) in the upstream region before interacting with the shock front (Figure 6d), during their first interaction with the shock front (Figure 6e), and when these are backstreaming into the upstream region after interacting with the shock front (Figure 6f). In order to extract this information, we have plotted the features of these particles as they come to the shock front and backstream at later times, but we do not integrate the trajectories in space or in time. In other words, we follow all these incoming ions and memorized their pitch angle when they are at a certain predetermined location (incoming upstream $D = 2000$ (Figure 6), at the shock front $D = 0$ (Figure 6e), and backstream upstream $D = 1000$ (Figure 6f)). This distance D is computed from the shock front, (more precisely from the middle of the ramp). As a consequence, each particle is not memorized at the same time or at the same θ_{Bn} location (only the distance D from the shock is fixed) and then, we record the behavior of all foreshock particles during the three stages of the reflection process.

Then, these plots represent the global behavior of the backstreaming ions as these interact with the shock front (independently of the sampling boxes). In the three panels, we continue to refer the two populations as FAB and GPB in order to be consistent throughout this paper but it is obvious that this classification is only clear at the end of the simulation when the backstreaming ions have been reflected back into the upstream region. Then, the FAB and GPB terms qualify their final distribution function and not the distribution plotted in this figure. As expected, the pitch angle distribution for both populations (FAB and GPB) looks similar before ions interact with the front ($0° \leq \alpha_o \leq 180°$). Only the amplitudes of $f(\alpha)$ are different because the FAB population is dominant everywhere within the ion foreshock as already pointed out in section 3.1. Indeed, larger parallel energy is gained after several bounces (i.e., FAB particles) than after only one (i.e., GPB particles) (see *Savoini et al.* [2013] for details).

More surprising is the Figure 6e defined when particles hit for the first time the shock front (i.e., $D = 0$) where both FAB and GPB populations exhibit the same pitch angle distribution centered around $\alpha \approx 30°$. Both distributions are shrinked since they suffer the same parallel acceleration (with $E_{//}$) and the same perpendicular drift (i.e., $\vec{E} \times \vec{B}$ drift). This result indicates that both backstreaming populations have exactly the same formation mechanism or, in other words, the same origin within the shock front. Finally, Figure 6f recovers the well-known pitch angle distributions for FAB (i.e., centered around 0°) and GPB (i.e., centered around 30°)

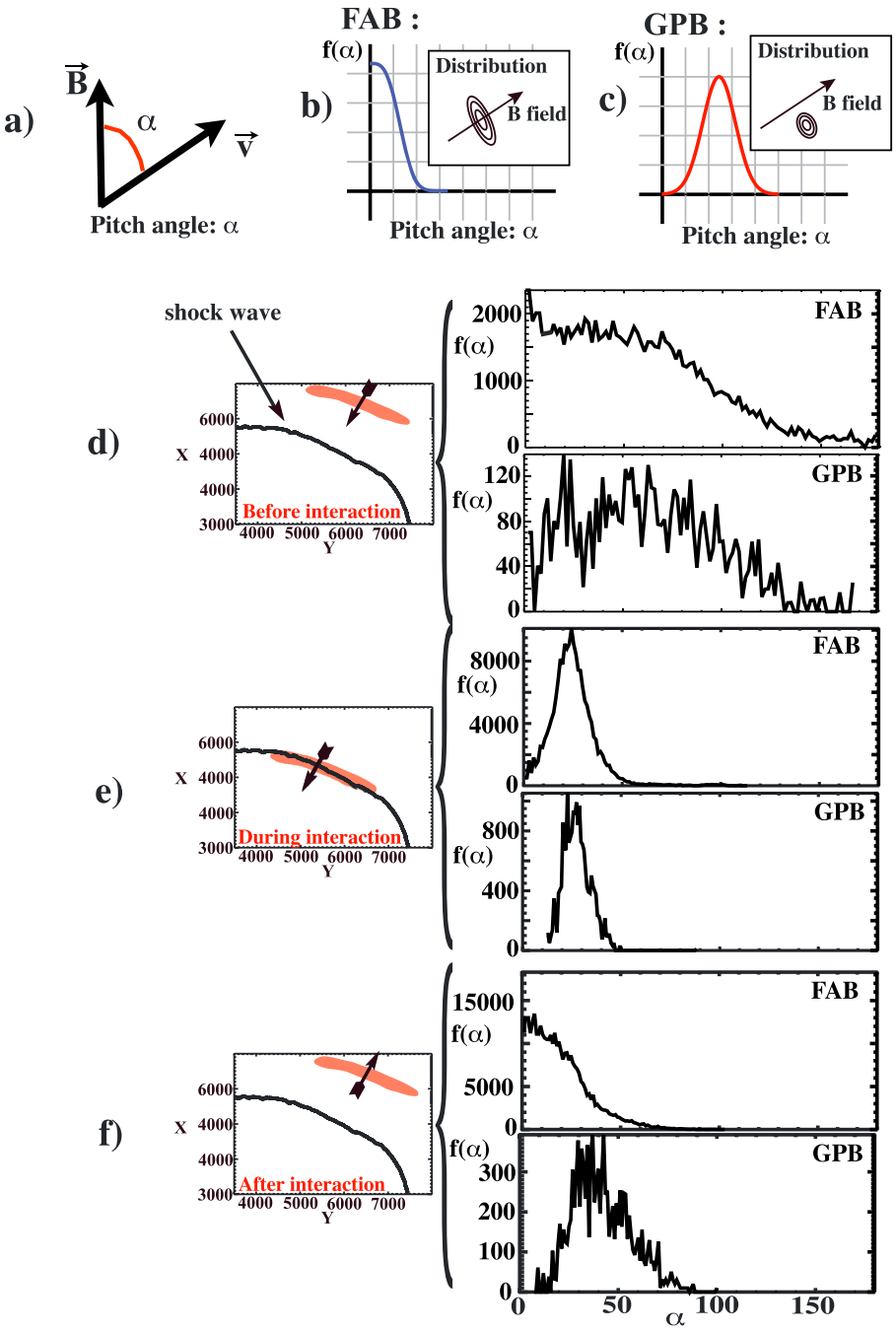

Figure 6. (a–c) The pitch angle α (defined by $\vec{v} \cdot \vec{B} = vB\cos(\alpha)$) and the sketches of pitch angle ion distributions $f(\alpha)$ for FAB and GPB populations, respectively. Following panels represent distributions $f(\alpha)$ for each population measured for the whole ion foreshock, at three different positions during the simulation: namely, (d) when ions are in the upstream region (i.e., before the shock interaction, at $\tilde{D} = 2000$), (e) at the front shock, (i.e., during the first hit of ions with the shock front at $\tilde{D} = 0$;), and finally, (f) when same ions are backstreaming into the upstream region (i.e., after interaction with the front at $\tilde{D} = 1000$).

when particles backstream into the ion foreshock. Then, while the GPB population conserves their nonzero pitch angle around 30° for all θ_{Bn} presently considering, with only a slight enlargement of its distribution (i.e., there is some phase mixing), the FAB ions lose their phase coherency and recover a gyrotropic distribution with a pitch angle α around 0°. These results illustrate the consequences of the scenario described in *Savoini et al.* [2013] where FAB ions suffer several bounces on the shock front and then, gain a random phase in perpendicular velocity as they meet different shock profiles (the amplitude of magnetic and electric fields varies

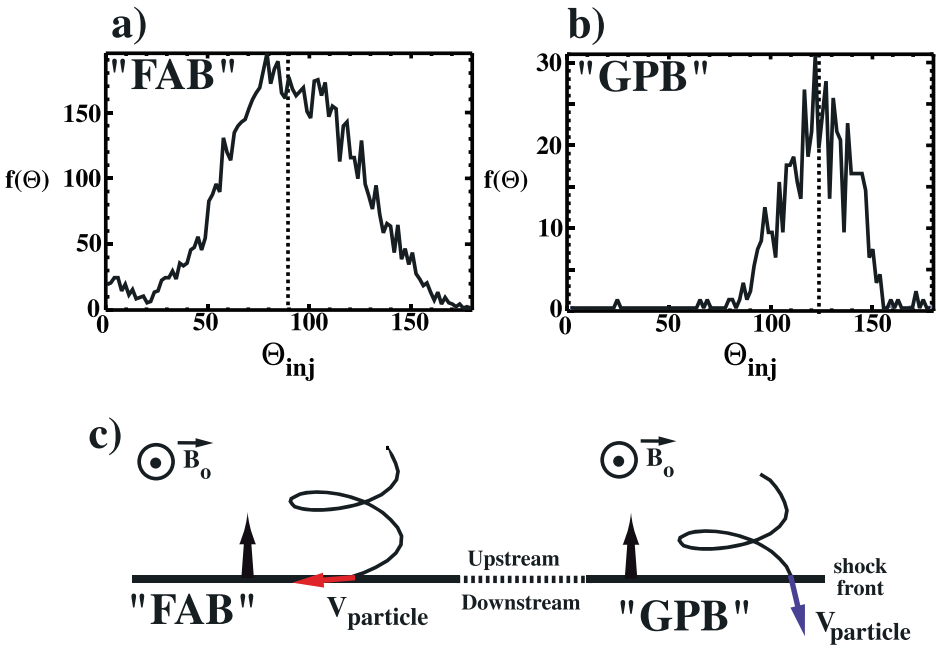

Figure 7. Ion distribution of the injection angle computed between the local normal of the shock front (at $\tilde{D} = 0$) and the ion velocity projected within the simulation plane (i.e., $\vec{v}_{XY} \cdot \vec{n} = v_{XY} n \cos(\theta_{\text{inj}})$, measured for FAB and the GPB populations, respectively. For reference, (c) corresponding trajectories in the *XY* space.

versus θ_{Bn} and in time because of nonstationary effects), whereas GPB ions after only one bounce do not suffer any noticeable change in their pitch angle distribution and stay aggregated as in Figure 5.

With this result in mind, it is simple to understand the *ring shape* of the FAB velocity distributions observed at the leading edge of the ion foreshock (in boxes 1, 4, and 7 of Figure 4). Indeed, these boxes collect only ions freshly reflected by the shock front and so, the number of bounces are limited to 2–3 which is not large enough to get a noticeable phase mixing. Then, we observe, here, the intermediate state of the formation of the FAB population.

4. Discussion

At this stage, a question arises: if the final state of backstreaming ions does not depend of their initial velocity features, how and why the incoming ion population is split into two distinct groups after interaction? Obviously, the most relevant explanation must involve the interaction time criterion Δt_{int} used in order to discriminate between both populations.

4.1. Injection Angle Dependence

In order to answer this question, we have plotted in Figure 7, the ion distribution function versus their injection angle θ_{inj} defined between the incoming upstream ion velocity vector $\vec{v}_{XY}$ projected into the simulation plane and the normal to the shock front $\vec{n}$, for all particles selected in the box 2.

$$\theta_{\text{inj}} = \arccos\left(\frac{v_x \cdot n_x + v_y \cdot n_y}{\|\vec{v}_{XY}\| \cdot \|\vec{n}\|}\right) \tag{4}$$

We consider the $\vec{v}_{XY}$ vector since the normal, $\vec{n}$, is only defined within the plane *XY* (it is a 2-D simulation). This angle provides informations on how ions interact locally with the shock front when these hit it. More precisely, the θ_{inj} is identified when the particle hits the middle of the shock ramp defined by $D = 0$. Figure 7a plots the distribution of $\theta_{\text{inj}}^{\text{FAB}}$ which shows clearly a maximum around $\theta_{\text{inj}}^{\text{FAB}} \approx 90°$, meaning that most of the future incoming FAB particles are injected with a velocity almost aligned along the shock front (i.e., perpendicular to $\vec{n}$). In contrast, Figure 7b evidences that the distribution of $\theta_{\text{inj}}^{\text{GPB}}$ has a maximum around 130° but more important, there no GPB particles having θ_{inj} below or equal to 90°; GPB are injected with a velocity almost (but not exactly) along the shock normal. As an illustration, a sketch of their individual trajectories has been

plotted in Figure 7c showing the typical distinct injection angles which discriminate the two backstreaming populations. Obviously, both populations need to have specific encounter with the shock front to be reflected. At this point, it is important to emphasize that the difficulties to compute exactly the local shock normal for each particle can lead to an enlargement of the distribution, and then only the statistical distribution of θ_{inj} has a physical meaning.

4.2. Origin of Bunched Distributions

Then, we evidenced that both populations have the same initial reflection process and only their particular injection angle can explain their different time history (i.e., one or several bounces on the shock front) leading to the generation of FAB or GPB populations. This surprising result can be explained in terms of electric field interaction. Indeed, in absence of instabilities, only two distinct processes may modify the pitch angle distribution: (i) a parallel acceleration by the macroscopic electrostatic component $\tilde{E}_{l\|}$ present at the front which increases the parallel velocity but not its perpendicular component or (ii) a perpendicular velocity drift (the $\tilde{E}_l \times \tilde{B}$ drift), responsible for the bunched perpendicular velocity distribution [*Gurgiolo et al.*, 1981]. Theoretically, this last point can be easily checked by computing the velocity drift and its associated pitch angle in our simulation for both populations. In normalized units, one gets

$$\alpha_{the} = \arctan\left(\frac{v_\perp}{v_\|}\right) = \arctan\left(\tilde{c}\frac{\tilde{E}_l \times \tilde{B}}{v_\| \tilde{B}^2}\right) \tag{5}$$

where $\tilde{E}_l$ and $\tilde{B}$ are the local electric and magnetic fields seen by ions when they are "injected" into the shock front (all computations are made within the solar wind reference frame). Figure 8 plots the distribution of associated theoretical pitch angle α_{theory} (equation (5)) to be compared with the numerical pitch angle distributions directly measured in the simulations (Figure 6e). In Figure 6e, we have used the definition $\alpha = \arcsin\left(v_\perp/v\right)$ where $v_\perp$ is the local ion perpendicular velocity. This allows us to compare precisely the perpendicular drift obtained in the two cases (i.e., $v_\perp$ from simulation and $v_\perp$ from the $\vec{E}_l \times \vec{B}$ drift, respectively). Figure 8 provides two important clues to understand the future of the backstreaming ions. First, the pitch angle of the GPB population is exactly determined by the $\vec{E} \times \vec{B}$ drift at the shock front as described by *Gurgiolo et al.* [1981]'s scenario. Second, the "theoretical" pitch angle distribution is very similar for both FAB and GPB populations, a feature which was not expected. An identical pitch angle distribution $f(\alpha)$ (i.e., same mean value $< \alpha >_{mean} \approx 30°$ with the same standard deviation $\sigma \approx 20°$) strongly suggests, once again, that the reflection mechanism is the same for both populations (i.e., same $v_\|$ and $v_\perp$ velocity evolution). In other words, particles split into two distinct populations only because FAB suffer several bounces on the shock front and that, without invoking other complex mechanisms.

4.3. Gain of Parallel Energy

In fact, a simple picture of this behavior is that of a *surfer* who moves with the flow to ride the large-amplitude wave. FAB ions follow very similar trajectories with the shock front. Such a surfing mechanism has been already described in the literature [*Shapiro*, 2003; *Kichigin*, 2009; *Lever et al.*, 2001] where ions are reflected back into the upstream region by the shock potential (or in other words, by the electrostatic field present at the ramp) but return to the shock front by the Lorentz force. In the present case, the process repeats until the ions gain enough energy to escape from the front.

Unfortunately, a further analysis of this mechanism is out of scope of the present paper since it requires to investigate individual trajectories in order to determine precisely the acceleration process related to the FAB population.

The behavior of GPB ions is totally different since these hit the shock front nearly along the normal and then, have to turn back before escaping into the upstream region and do not make any further interaction with the shock wave. In other words, they stay around $\frac{1}{2}\tau_{ci}$ in the shock front (i.e., an half period) to compare with the FAB ions which need less time ($\frac{1}{4}\tau_{ci}$) before escaping from the shock front. Then, one can roughly estimate the difference of parallel energy gain between the two populations during their first encounter with the shock front by assuming that both populations see the same shock front profile (in terms of macroscopic magnetic and electric fields at the ramp).

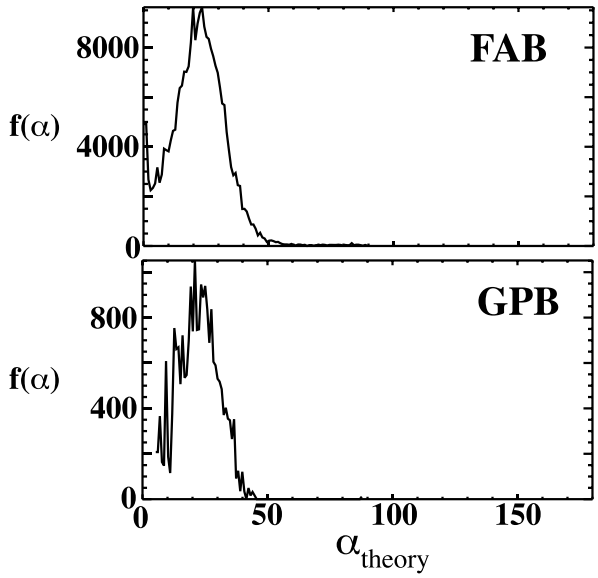

Figure 8. Pitch angle ion distributions based on the theoretical pitch angle α_{the} (see equation (5)) computed as incoming ions hit the shock front (at $\tilde{D} = 0$) for FAB and GPB population, respectively. This figure has to be compared with Figure 6e.

In these conditions, the differential acceleration between FAB and GPB particles depends only on the time spent in the parallel electric field (i.e., we have $dv_{\parallel} = \frac{q}{m} E_{\parallel} dt$). Then, we find the simple relation.

$$\frac{\Delta v_{\parallel}^{GPB}}{\Delta v_{\parallel}^{FAB}} \approx 2 \tag{6}$$

We have to limit our estimate to this ratio since the time and space fluctuations of the electric field seen by the particles differ, and then, do not allow a clear comparison between both populations. Nevertheless, equation (6) emphasizes that a GPB particle gains twice the energy of the FAB particle during the "first" bounce. In other words, the energy gain is large enough for both populations to be reflected by the shock front. More precisely, the FAB particles have gained just enough parallel energy to go into the upstream region but must return to the front during the second part of their gyration (multibounces behavior characteristic of the FAB population). In contrast, GPB particles gain enough parallel energy during their first bounce so that their guiding center frame definitively escapes into the upstream region, and then, a single bounce characterizes this population.

5. Conclusions

In a previous paper, *Savoini et al.* [2013] have stressed out that a simple criterion (the interaction time range Δt_{int}) allows to clearly distinguish the FAB and GPB distributions. In complement, the present paper uses this criterion to provide some clues to analyze in more details the ion reflection processes at the shock front. In particular, four main points have been evidenced:

1. Both FAB and GPB populations can be produced by the shock front itself. Our results demonstrate that both populations may have the same origin, a perpendicular acceleration related to the electrostatic field present at the ramp. Following *Gurgiolo et al.* [1981], we see that the $\vec{E} \times \vec{B}$ drift can account for the pitch angle distribution observed at the shock front for each population. Indeed, the comparison of Figures 8 and 6e shows a very good agreement between our simulation results and the theoretical pitch angle distribution computed with the help of $\vec{E} \times \vec{B}$ drift. At this point, one can emphasize that near the leading edge of the ion foreshock (i.e., for $\theta_{Bn} \geq 66°$, boxes 1, 4, and 7 of Figure 4), we observe only the early steps of the formation of a random perpendicular velocity distribution because these particles are hit by the shock front nearly at the end of the simulation and only suffer 2–3 bounces which is not enough to get a noticeable phase mixing.

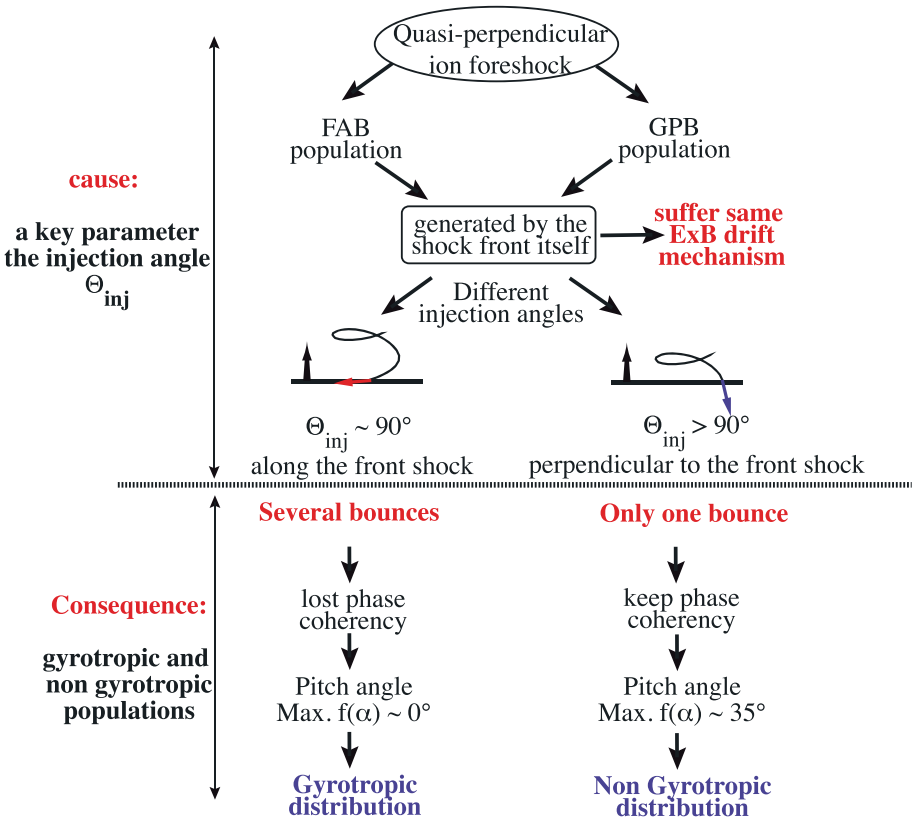

Figure 9. Schematic diagram of the scenario of processes described in this paper for the formation of the quasi-perpendicular ion foreshock.

2. As already pointed out by *Savoini et al.* [2013], the FAB and GPB populations coexist deeply into the foreshock which is understandable if one recalls that these are coming from the same region and suffer the same reflection mechanism at the front. Then, new criteria have been necessary in order to distinguish both populations as incoming ions hit the shock front. Present statistical study on the injection angle θ_{inj} (defined between the shock normal direction and the ion gyrating velocity vector projected into the simulation plane.) has shown that backstreaming ions are classified as FAB particles if these are injected almost along the shock front ($\theta_{inj} \approx 90°$), while GPB particles are injected almost along the shock normal (θ_{injs} is larger than 90°). This result has one main consequence: no specific initial condition needs to be satisfied for the solar wind incoming ions in terms of energy, velocity distribution, or pitch angle. Only the very local interaction with the shock front in time and in space is responsible for the future of such particles.
3. Our simulations have pointed out that the time evolution of the shock front itself has important consequences on the backstreaming populations and leads to a *nonstationary* reflection process. Indeed, we have evidenced that the reflection process (for both FAB and GPB population) is much more efficient when the magnetic foot/emitted whistler precursor has reached an amplitude comparable to the overshoot during the cyclic reformation (i.e., only the ramp is visible). Then, the associated electric field is maximum and acts as the source formation of both backstreaming populations.
4. At least, the differences observed between FAB and GPB populations do not involve some distinct reflection processes as often claimed in the literature but follow from the particles time history at the shock front. *Both FAB and GPB ions suffer the same reflection process and have the same nongyrotropic distribution but only FAB population loose their initial phase coherency by suffering several bounces*. This important result was not expected and greatly simplifies the question of their origin. Figure 9 illustrates schematically present conclusions concerning the origin of the quasi-perpendicular ion foreshock.

Of course, our results do not take into account instabilities which can relax (and destroy) these particular distributions out of equilibrium as well as the phase mixing over long distances. Present mechanisms apply to conditions where ion instabilities are excluded and for distances relatively short from the shock front 2–3 R_E.

However, these do not eliminate other possible mechanisms proposed to account for the generation of the nongyrotropic population. In particular, several works have been done on beam-plasma instabilities which can lead to a conversion of the field-aligned beams to gyrophase bunched populations [*Hoshino and Terasawa*, 1985; *Mazelle et al.*, 2003; *Meziane*, 2005; *Mazelle et al.*, 2005; *Kis et al.*, 2007]. Such a wave-trapping process does not occur in our simulation since its wave growth rate is too small compared to the simulation time [*Gary*, 1981] but can explain the gyrophase bunched distribution observed far from the shock ($> 10\ R_E$).

Last but not least, no clear simultaneously observations of FAB and GPB populations have been clearly reported in the literature. Such lack of simultaneous observations may have been the result of the difficulties to clearly separate the two ion components near the shock front as already pointed out by *Savoini et al.* [2013] who have shown the necessity for using more refined criteria to identify each population. Within this context, let us precise that *Meziane et al.* [2004b] have reported on observations of briefly overlapping field-aligned and gyrating ion populations, in a region upstream of the Earth's bow shock. Nevertheless, no clear production mechanism has been established. Our simulation results could be proposed to explain these observations, even if there are localized at the edge of the ion foreshock which is not the case in this paper.

Acknowledgments

The numerical simulations described in this paper were performed on the supercomputer center "IDRIS" institute of the Centre National de la Recherche Scientifique (CNRS) (http://www.idris.fr). This work received financial support by the program "Investissements d'avenir" under the reference ANR-11-IDEX-0004-02 (Plas@Par). Data supporting this study may be accessible at (http://www.lpp.fr) by contacting the authors. Thanks must be addressed to Jean-Noel Leboeuf for having provided the basic (periodic) version of the 2-D code.

Michael Balikhin thanks Christian Mazelle and William Wilkinson for their assistance in evaluating this paper.

References

Bale, S., et al. (2005), Quasi-perpendicular shock structure and processes, *Space Sci. Rev.*, *118*, 161–203, doi:10.1007/s11214-005-3827-0.

Bonifazi, C., and G. Moreno (1981a), Reflected and diffuse ions backstreaming from the Earth's bow shock: 2. Origin, *J. Geophys. Res.*, *86*(A6), 4405–4413.

Bonifazi, C., and G. Moreno (1981b), Reflected and diffuse ions backstreaming from the Earth's bow shock: 1. Basic properties, *J. Geophys. Res.*, *86*(A6), 4397–4404.

Eastwood, J., E. Lucek, C. Mazelle, and K. Meziane (2005), The foreshock, *Space Sci. Rev.*, *118*, 41–94, doi:10.1007/s11214-005-3824-3.

Edmiston, J. P., C. F. Kennel, and D. Eichler (1982), Escape of heated ions upstream of quasi-parallel shocks, *Geophys. Res. Lett.*, *9*, 531–534, doi:10.1029/GL009i005p00531.

Fuselier, S. A. (1995), Ion distributions in the Earth's foreshock upstream from: The bow shock, *Adv. Space Res.*, *15*(8/9), 43–52.

Fuselier, S. A, M. Thomsen, and J. Gosling (1986), Gyrating and intermediate ion distributions upstream from the Earth's bow shock, *J. Geophys. Res.*, *91*(A1), 91–99.

Gary, S. P. (1981), Microinstabilities upstream of the Earth's bow shock—A brief review, *J. Geophys. Res.*, *86*, 4331–4336, doi:10.1029/JA086iA06p04331.

Giacalone, J., J. R. Jokipii, and J. Kota (1994), Ion injection and acceleration at quasi-perpendicular shocks, *J. Geophys. Res.*, *99*(A10), 19,351–19,358.

Gosling, J. T., M. F. Thomsen, S. J. Bame, W. C. Feldman, G. Pashmann, and N. Sckopke (1982), Evidence for specularly reflected ions upstream from the quasi-parallel bow shock, *Geophys. Res. Lett.*, *9*, 1333–1336.

Gurgiolo, C., G. K. Parks, B. H. Mauk, K. A. Anderson, R. P. Lin, H. Reme, and C. S. Lin (1981), Non-E × B ordered ion beams upstream of the Earth's bow shock, *J. Geophys. Res.*, *86*(A6), 4415–4424, doi:10.1029/JA086iA06p04415.

Gurgiolo, C., G. Parks, and G. Mauk (1983), Upstream gyrophase bunched ions—A mechanism for creation at the bow shock and the growth of velocity space structure through gyrophase mixing, *J. Geophys. Res.*, *88*(A11), 9093–9100.

Hamza, A. M., K. Meziane, and C. Mazelle (2006), Oblique propagation and nonlinear wave particle processes, *J. Geophys. Res.*, *111*, A04104, doi:10.1029/2005JA011410.

Horbury, T. S., E. A. Lucek, A. Balogh, M. W. Dunlop, T. M. Oddy, C. Carr, P. Brown, A. Szabo, and K.-H. Fornacon (2001), Cluster magnetic field observations of the bowshock: Orientation, motion and structure, *Ann. Geophys.*, *19*, 1399–1409.

Hoshino, M., and T. Terasawa (1985), Numerical study of the upstream wave excitation mechanism: 1. Nonlinear phase bunching of beam ions, *J. Geophys. Res.*, *90*(A1), 57–64.

Kichigin, G. N. (2009), On the origin of energetic particles in the foreshock region of the Earth's bow shock, *Astron. Lett.*, *35*, 261–269, doi:10.1134/S1063773709040069.

Kis, A., M. Scholer, B. Klecker, H. Kucharek, E. A. Lucek, and H. Rème (2007), Scattering of field-aligned beam ions upstream of Earth's bow shock, *Ann. Geophys.*, *25*, 785–799.

Kucharek, H. (2008), On the physics of collisionless shocks: Cluster investigations and simulations, *J. Atmos. Sol. Terr. Phys.*, *70*, 316–324, doi:10.1016/j.jastp.2007.08.052.

Kucharek, H., E. Möbius, M. Scholer, C. Mouikis, L. Kistler, T. Horbury, A. Balogh, H. Réme, and J. Bosqued (2004), On the origin of field-aligned beams at the quasi-perpendicular bow shock: Multi-spacecraft observations by Cluster, *Ann. Geophys.*, *22*, 2301–2308.

Lee, R., and S. Chapman (2005), Reforming perpendicular shocks in the presence of pickup protons: Initial ion acceleration, *Ann. Geophys.*, *23*(2), 643–650.

Lefebvre, B., Y. Seki, S. J. Schwartz, C. Mazelle, and E. A. Lucek (2010), Reformation of an oblique shock observed by Cluster, *J. Geophys. Res.*, *114*, A11107, doi:10.1029/2009JA014268.

Lembege, B., and J. M. Dawson (1987), Self-consistent study of a perpendicular collisionless and nonresistive shock, *Phys. Fluids*, *30*, 1767, doi:10.1063/1.866191.

Lembege, B., and P. Savoini (1992), Nonstationarity of a two-dimensional quasiperpendicular supercritical collisionless shock by self-reformation, *Phys. Fluids*, *4*(11), 3533–3548.

Lembege, B., and P. Savoini (2002), Formation of reflected electron bursts by the nonstationarity and nonuniformity of a collisionless shock front, *J. Geophys. Res.*, *107*, 1037, doi:10.1029/2001JA900128.

Lembege, B., J. Giacalone, M. Scholer, T. Hada, M. Hoshino, V. Krasnosel'skikh, H. Kucharek, P. Savoini, and T. Terasawa (2004), Selected problems in collisionless-shock physics, *Space Sci. Rev.*, *110*(3/4), 161–226, doi:10.1023/B:SPAC.0000023372.12232.b7.

Leroy, M. M., and A. Mangeney (1984), A theory of energization of solar wind electrons by the Earth's bow shock, *Ann. Geophys.*, *2*(4), 449–456.

Lever, E. L., K. B. Quest, and V. D. Shapiro (2001), Shock surfing vs. shock drift acceleration, *Geophys. Res. Lett.*, *28*, 1367–1370, doi:10.1029/2000GL012516.

Lobzin, V. V., V. V. Krasnoselskikh, J.-M. Bosqued, J.-L. Pinçon, S. J. Schwartz, and M. Dunlop (2007), Nonstationarity and reformation of high-Mach-number quasiperpendicular shocks: Cluster observations, *Geophys. Res. Lett.*, *34*, L05107, doi:10.1029/2006GL029095.

Mazelle, C., et al. (2003), Production of gyrating ions from nonlinear wave-particle interaction upstream from the Earth's bow shock: A case study from Cluster-CIS, *Planet. Space Sci.*, *51*, 785–795, doi:10.1016/S0032-0633(03)00107-7.

Mazelle, C., K. Meziane, and M. Wilber (2005), Field-aligned and gyrating ion beams in a planetary foreshock, *AIP Conf. Proc.*, *781*, 89–94, doi:10.1063/1.2032680.

Mazelle, C., et al. (2010), Self-reformation of the quasi-perpendicular shock: CLUSTER observations, in *Twelfth International Solar Wind Conference*, *AIP Conf. Proc.*, *1246*, 471–474, doi:10.1063/1.3395905.

Meziane, K. (2005), A review of field-aligned beams observed upstream of the bow shock, in *The Physics of Collisionless Shocks: 4th Annual IGPP International Astrophysics Conference*, *AIP Conf. Proc.*, *781*, 116–122, doi:10.1063/1.2032683.

Meziane, K., C. Mazelle, R. P. Lin, D. Lequéau, D. E. Larson, G. K. Parks, and R. P. Lepping (2001), Three-dimensional observations of gyrating ion distributions far upstream from the Earth's bow shock and their association with low-frequency waves, *J. Geophys. Res.*, *106*(A4), 5731–5742, doi:10.1029/2000JA900079.

Meziane, K., et al. (2004a), Bow shock specularly reflected ions in the presence of low-frequency electromagnetic waves: A case study, *Ann. Geophys.*, *22*, 2325–2335.

Meziane, K., et al. (2004b), Simultaneous observations of field-aligned beams and gyrating ions in the terrestrial foreshock, *J. Geophys. Res.*, *109*, A05107, doi:10.1029/2003JA010374.

Meziane, K., A. M. Hamza, M. Wilber, M. A. Lee, C. Mazelle, E. A. Lucek, and T. Hada (2011), Specular refection at a non-stationary shock: A simple model, *Planet. Space Sci.*, *59*, 495–501, doi:10.1016/j.pss.2010.10.016.

Möbius, E., et al. (2001), Observations of the spatial and temporal structure of field-aligned beam and gyrating ring distributions at the quasi-perpendicular bow shock with Cluster CIS, *Ann. Geophys.*, *19*, 1411–1420.

Moullard, O., D. Burgess, T. Horbury, and E. Lucek (2006), Ripples observed on the surface of the Earth's quasi-perpendicular bow shock, *J. Geophys. Res.*, *111*, A09113, doi:10.1029/2005JA011594.

Oka, M., T. Terasawa, Y. Saito, and T. Mukai (2005), Field-aligned beam observations at the quasi-perpendicular bow shock: Generation and shock angle dependence, *J. Geophys. Res.*, *110*, A05101, doi:10.1029/2004JA010688.

Paschmann, G., N. Sckopke, and J. Asbridge (1980), Energization of solar wind ions by reflection from the Earth's bow shock, *J. Geophys. Res.*, *85*(A9), 4689–4693.

Paschmann, G., N. Sckopke, J. R. Asbridge, S. J. Bame, and J. T. Gosling (1981), Characteristics of reflected and diffuse ions upstream from the Earth'bow shock, *J. Geophys. Res.*, *86*, 4355–4364.

Paschmann, G., N. Sckopke, S. J. Bame, and J. T. Gosling (1982), Observations of gyrating ions in the foot of the nearly perpendicular bow shock, *Geophys. Res. Lett.*, *9*, 881–884.

Savoini, P., and B. Lembège (2001), Two-dimensional simulations of a curved shock: Self-consistent formation of the electron foreshock, *J. Geophys. Res.*, *106*, 12,975–12,992, doi:10.1029/2001JA900007.

Savoini, P., B. Lembege, and J. Stienlet (2010), Origin of backstreaming electrons within the quasi-perpendicular foreshock region: Two-dimensional self-consistent PIC simulation, *J. Geophys. Res.*, *115*, A09104, doi:10.1029/2010JA015263.

Savoini, P., B. Lembege, and J. Stienlet (2013), On the origin of the quasi-perpendicular ion foreshock: Full-particle simulations, *J. Geophys. Res. Space Physics*, *118*, 1132–1145, doi:10.1002/jgra.50158.

Scholer, M., and S. Matsukiyo (2004), Nonstationarity of quasi-perpendicular shocks: A comparison of full particle simulations with different ion to electron mass ratio, *Ann. Geophys.*, *22*, 2345–2353, doi:10.5194/angeo-22-2345-2004.

Schwartz, S. J., and D. Burgess (1984), On the theoretical/observational comparison of field-aligned ion beams in the Earth's foreshock, *J. Geophys. Res.*, *89*, 2381–2384, doi:10.1029/JA089iA04p02381.

Schwartz, S. J., M. F. Thomsen, and J. T. Gosling (1983), Ions upstream of the Earth's bow shock: A theoretical comparison of alternative source populations, *J. Geophys. Res.*, *88*(A3), 2039–2047, doi:10.1029/JA088iA03p02039.

Shapiro, V. D. (2003), Shock surfing acceleration, *Planet. Space Sci.*, *51*, 665–680, doi:10.1016/S0032-0633(03)00102-8.

Sonnerup, B. U. Ö. (1969), Acceleration of particles reflected at a shock front, *J. Geophys. Res.*, *74*(5), 1301–1304, doi:10.1029/JA074i005p01301.

Tanaka, M., C. C. Goodrich, D. Winske, and K. Papadopoulos (1983), A source of the backstreaming ion beams in the foreshock region, *J. Geophys. Res.*, *88*(A4), 3046–3054, doi:10.1029/JA088iA04p03046.

Thomsen, M., J. Gosling, and S. Bame (1985), Gyrating ions and large-amplitude monochromatic MHD waves upstream of the Earth's bow shock, *J. Geophys. Res.*, *90*(A1), 267–273.

Thomsen, M. F., J. T. Gosling, S. J. Bame, W. C. Feldman, G. Paschmann, and N. Sckopke (1983), Field-aligned ion beams upstream of the Earth's bow shock: Evidence for a magnetosheath source, *Geophys. Res. Lett.*, *10*(12), 1207–1210, doi:10.1029/GL010i012p01207.

Tsurutani, B. T., and P. Rodriguez (1981), Upstream waves and particles—An overview of ISEE results, *J. Geophys. Res.*, *86*, 4317–4324.

Yamauchi, M., et al. (2011), Comparison of accelerated ion populations observed upstream of the bow shocks at Venus and Mars, *Ann. Geophys.*, *29*, 511–528, doi:10.5194/angeo-29-511-2011.